Physics-based modelling and data-driven optimisation of a latent heat thermal energy storage system with corrugated fins

Tavakoli, Ali; Hashemi, Javad; Najafian, Mahyar; Ebrahimi, Amin

DOI
10.1016/j.renene.2023.119200

Publication date
2023

Document Version
Final published version

Published in
Renewable Energy

Citation (APA)
Tavakoli, A., Hashemi, J., Najafian, M., & Ebrahimi, A. (2023). Physics-based modelling and data-driven optimisation of a latent heat thermal energy storage system with corrugated fins. *Renewable Energy*, *217*, Article 119200. https://doi.org/10.1016/j.renene.2023.119200

Renewable Energy 217 (2023) 119200

Contents lists available at ScienceDirect

Renewable Energy

journal homepage: www.elsevier.com/locate/renene

Physics-based modelling and data-driven optimisation of a latent heat thermal energy storage system with corrugated fins

Ali Tavakoli [a], Javad Hashemi [a], Mahyar Najafian [a], Amin Ebrahimi [b,*]

[a] Department of Mechanical Engineering, Faculty of Engineering, Ferdowsi University of Mashhad, P.O. Box 91775-1111, Mashhad, Iran
[b] Department of Materials Science and Engineering, Faculty of Mechanical, Maritime and Materials Engineering, Delft University of Technology, Mekelweg 2, 2628CD, Delft, The Netherlands

ARTICLE INFO

Keywords:
Thermal energy storage system
Phase change material
Thermal and fluid flow modelling
Optimisation
Machine learning
Deep neural networks

ABSTRACT

Solid-liquid phase transformation of a phase change material in a rectangular enclosure with corrugated fins is studied. Employing a physics-based model, the influence of fin length, thickness, and wave amplitude on the thermal and fluid flow fields is explored. Incorporating fins into thermal energy storage systems enhances the heat transfer surface area and thermal penetration depth, accelerating the melting process. Corrugated fins generate more flow perturbations than straight fins, improving the melting performance. Longer and thicker fins increase the melting rate, average temperature, and thermal energy storage capacity. However, the effect of fin thickness on the thermal characteristics seems insignificant. Larger fin wave amplitudes increase the heat transfer surface area but disrupt natural convection currents, slowing the melting front progress. A surrogate model based on an artificial neural network in conjunction with the particle swarm optimisation is developed to optimise the fin geometry. The optimised geometry demonstrates a 43% enhancement in thermal energy storage per unit mass compared to the case with planar fins. The data-driven model predicts the liquid fraction with less than 1% difference from the physics-based model. The proposed approach provides a comprehensive understanding of the system behaviour and facilitates the design of thermal energy storage systems.

1. Introduction

Latent heat thermal energy storage (LHTES) systems are a type of thermal energy storage technology that store and release energy through the phase transition of a material [1–3], typically a phase change material (PCM), such as paraffin, salt hydrates, or eutectic mixtures [4]. During the charging process, the PCM absorbs heat and undergoes a phase change from solid to liquid or from liquid to gas, which allows the system to store large amounts of energy at a nearly constant temperature. Conversely, during discharge, the PCM solidifies or condenses and releases the stored energy, providing a continuous and stable source of thermal energy. LHTES systems have shown great potential for various applications, such as in solar thermal power plants [5,6], district heating [7,8], building HVAC systems [9,10], and battery thermal management systems [11,12], due to their high energy storage density, low maintenance requirements, and improved energy efficiency [3]. As the demand for sustainable and efficient energy solutions continues to grow, the development and optimisation of these systems are becoming increasingly important.

The development of LHTES systems faces several challenges that need to be addressed to optimise their performance and ensure their successful implementation [13]. One of the primary challenges is the selection of a suitable PCM with high energy storage densities, appropriate phase change temperatures, and long-term stability to meet the specific requirements of the application [14]. Another challenge is the integration of PCM into practical and efficient systems that can withstand repeated cycling without degradation [15,16]. Moreover, the thermal conductivity of PCM is generally low, which can limit the rate of energy transfer and reduce the overall efficiency of the system. To overcome these challenges, various strategies have been explored [17], such as using high-performance PCM (*e.g.* nanocomposite PCM) [18–20], optimising the storage system design [21–26], and employing encapsulation techniques [27–29].

Extended surfaces, commonly known as fins, have been widely used to optimise the storage system design and enhance the performance of LHTES systems. A comprehensive overview of the fin designs employed in the literature to improve the performance of latent heat thermal energy storage systems is presented by Ye et al. [26] and Zhang et al. [30].

* Corresponding author.
E-mail address: A.Ebrahimi@tudelft.nl (A. Ebrahimi).

https://doi.org/10.1016/j.renene.2023.119200
Received 31 May 2023; Received in revised form 25 July 2023; Accepted 18 August 2023
Available online 21 August 2023

Fins increase the surface area of the storage container, which generally improves the rate of heat transfer between the PCM and the surrounding environment, reduces the time required for charging and discharging, and improves the overall efficiency of the system [31–36]. Fins can be attached to the outer surface of the container or embedded within the PCM to create a composite material. Fins with different geometries and materials have been investigated to optimise their performance. For instance, triangular [37], rectangular [36], and helical [38] have been used within the PCM to improve heat transfer rates. Additionally, materials such as copper, aluminium, and stainless steel have been employed as fin materials due to their high thermal conductivity [26, 30]. However, embedding fins in LHTES systems may increase the complexity of the system design and require additional maintenance efforts [39] and can disrupt the molten material flow and convective heat transfer in the container [33]. Additionally, the use of fins may increase the risk of leakage or damage to the storage container due to the stress caused by thermal expansion and contraction [39]. Furthermore, if the fins are not properly designed, they may result in the formation of undesired thermal gradients within the PCM, leading to reduced efficiency and even material degradation [40]. Therefore, while fins can improve the performance of latent heat thermal energy storage systems, particular attention should be paid to their design, materials, and installation to minimize the potential drawbacks and ensure optimal system performance [41–43].

Physics-based computational modelling of melting and solidification is a powerful tool to design and optimise the fin geometry and configuration for LHTES systems. These models enable the prediction of the complex fluid flow, heat transfer, and solid-liquid phase transformations in LHTES and provide insights into the effects of fin design parameters on the system performance. For instance, several studies have employed computational modelling to optimise the design of fins embedded in a PCM for improving the thermal performance of LHTES systems [44–48]. Computational models can also be coupled with optimisation techniques, such as topology optimisation, to find the optimal fin design that minimises the cost or maximizes the efficiency of LHTES systems [34, 49–51]. While physics-based computational models are valuable tools for fin design optimisation in latent heat thermal energy storage systems, these models are often computationally expensive, particularly for three-dimensional problems with large domains and fine meshes, limiting their applicability for (near) real-time optimisation of LHTES systems.

Recent developments in data-driven models based on artificial neural networks (ANNs) and deep learning have shown great potential for optimising the design of fins in LHTES systems [52]. Deep learning, a subset of ANNs, uses multiple layers of neurons to extract features and learn hierarchical representations of the input data [53]. Deep learning can be used to optimise the design of fins by learning from large datasets of simulated or experimental data and identifying the most effective fin geometries and configurations for enhancing the performance of the thermal energy storage system [52]. Deep learning can also overcome some of the limitations of physics-based models by providing fast and accurate predictions without requiring explicit knowledge of the underlying physical mechanisms [54]. Moreover, deep learning can capture complex and non-linear relationships between the design variables and the system performance that may be difficult to model using conventional physics-based approaches. Several recent studies have demonstrated the potential of ANNs and deep learning for fin design optimisation in latent heat thermal energy storage systems. For instance, Ermis et al. [55] developed a feed-forward back-propagation artificial neural network with three layers, an input layer, a hidden layer, and an output layer. They trained the ANN model using an experimental dataset and predicted the total stored energy and Nusselt number in a finned-tube thermal energy storage system for different operating conditions and fin parameters. Using a similar approach, Motahar [56] developed an ANN model to predict the Nusselt number and the volume fraction of molten material in a rectangular enclosure subjected to a uniform heat flux. In a recent study, Darvishvand et al. [33] performed physics-based numerical simulations to investigate the effects of fin height and number on the unsteady melting process of PCM in an LHTES system with rectangular enclosures. Using the outcomes of the simulations, they trained an ANNs model to correlate the instantaneous liquid fractions and stored energy in the system to the fin design parameters.

The solid-liquid phase transformation of a phase change material (RT82) in a latent heat thermal energy storage (LHTES) system with corrugated fins is studied in the present work. A physics-based computational model is developed to simulate the transient thermal and fluid flow fields in a rectangular enclosure with corrugated fins varying in length, amplitude, and thickness. The effect of fin geometries on the heat transfer performance and energy storage capacity of the LHTES system is thoroughly analysed using the physics-based model. To enhance the computational efficiency and reduce the computational cost associated with fin design optimisation, a feed-forward neural network (FFNN) is constructed as a surrogate model. The surrogate data-driven model correlates the instantaneous liquid fraction, energy stored in the system, and fin design parameters. The particle swarm optimisation (PSO) technique is applied to explore the design space and identify the optimal fin geometry that minimises the LHTES system charging time. The combination of the physics-based model, surrogate data-driven model, and optimisation techniques represents a promising approach for enhancing the performance of LHTES systems. The present work provides a systematic and robust methodology for designing and optimising LHTES systems with fins, which can improve their applicability in various thermal energy applications. The results of this work also contribute to advancing the fundamental understanding of phase change phenomena within LHTES systems, leading to more efficient and reliable thermal energy storage technologies.

2. Problem description

The evolution of thermal and fluid flow fields during the solid-liquid phase transformation of a phase change material (Rubitherm RT82) in a rectangular enclosure equipped with three equally spaced corrugated fins is studied in the present work. The schematic of the problem is shown in Fig. 1, where the enclosure has a length (L_e) of 120 mm and a height (H_e) of 50 mm. Fig. 1 also shows the boundary conditions employed in the simulations. The bottom surface of the enclosure is subjected to a constant temperature of T_w, while the other outer walls are thermally insulated. The corrugated fins are made of copper and have a sinusoidal shape, which is defined by three parameters: the fin

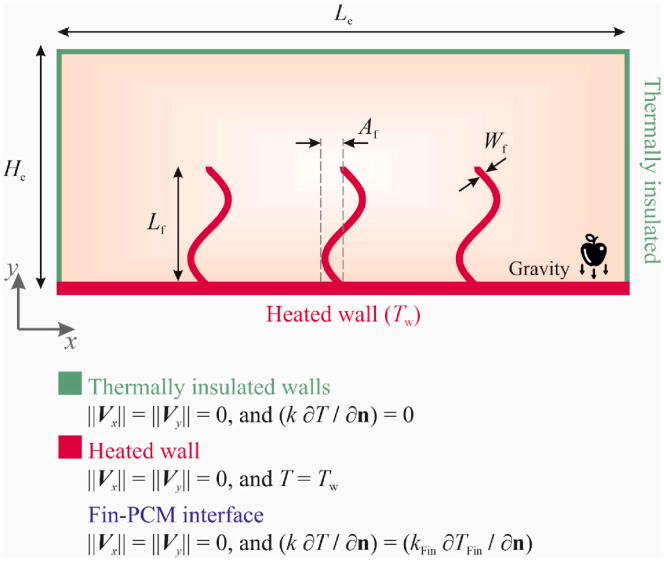

Fig. 1. Schematic of the thermal energy storage unit with three corrugated fins.

length L_f, the wave amplitude A_f, and the fin thickness W_f. Table 1 provides the thermophysical properties of both Rubitherm RT82 and copper utilised in the simulations, which were obtained from Refs. [57, 58].

The phase change material in the enclosure has an initial temperature (T_i) of 300.15 K, which is lower than its melting temperature. The simulation involves the sudden increase of temperature of the heated wall to a value above the melting temperature of the phase change material (T_w = 363.15 K) to replicate the charging process. Subsequently, the temperature of the heated wall is decreased to its initial value ($T_w = T_i$ = 300.15 K) to simulate the discharging process. In the simulations, the solid walls are modelled as no-slip walls. Simulations are conducted to investigate the impact of fin design on the performance of system. A well-structured design of experiment (DoE) was constructed using the Design Expert software to efficiently and systematically explore the effects of geometrical variables on the system's performance. The Box-Behnken design method from the response surface methodology (RSM) category of DoE was employed for this purpose. The design space was bounded by the ranges [20, 40 mm], [5, 15 mm] and [1, 3 mm] for length, wave amplitude, and thickness of the fins respectively. Table 2 presents a summary of the cases the cases that were simulated using the physics-based model.

3. Physics-based model

The physics-based computational model is constructed based on the finite-volume method within the framework of ANSYS Fluent to study the two-dimensional heat and molten material flow during charging and discharging processes. The molten material is modelled as Newtonian and incompressible, while the flow in the enclosure is assumed to be laminar. Thermal buoyancy effects are incorporated into the model using the Boussinesq assumption [59]. Melting and solidification of the phase change material are modelled using the enthalpy-porosity method [60]. Accordingly, the unsteady equations governing the conservation of mass, momentum, and energy are formulated respectively as follows:

$$\nabla \bullet \boldsymbol{V} = 0, \tag{1}$$

$$\frac{\partial}{\partial t}(\rho \boldsymbol{V}) + \nabla \bullet (\rho \boldsymbol{V}\boldsymbol{V}) = \mu \nabla^2 \boldsymbol{V} - \nabla p + \rho \beta \boldsymbol{g}(T - T_r) - C\frac{(1-\lambda)^2}{\lambda^3 + \varepsilon}\boldsymbol{V}, \tag{2}$$

$$\frac{\partial}{\partial t}(\rho H) + \nabla \bullet (\rho \boldsymbol{V} H) = \nabla \bullet (k \nabla T), \tag{3}$$

where $\boldsymbol{V}$ is the velocity vector, t is the time, ρ is the density, μ is the dynamic viscosity, p is the pressure, β is the thermal expansion coefficient, $\boldsymbol{g}$ is the gravitational acceleration vector, T is the temperature, T_r is the reference temperature, C is the mushy-zone constant, ε is a constant equal to 10^{-3}, H is the total enthalpy of the material, and k is the thermal conductivity. The value of the mushy-zone constant is set to 10^7 kg m^{-2} s^{-2}, according to the criterion suggested by Ebrahimi et al. [61]. The total enthalpy of the material (H) is the sum of the sensible heat (H_s) and the latent heat (H_l), and is defined as follows [62]:

$$H = H_s + H_l = \left(h_r + \int_{T_r}^{T} c_p \mathrm{d}T\right) + \lambda H_f. \tag{4}$$

Here, h_r is the enthalpy of the material at the reference temperature T_r, c_p is the specific heat capacity, H_f is the latent heat of fusion, and λ is the local liquid fraction. The value of the local liquid fraction λ is assumed to depend on temperature only and is defined as follows [62]:

$$\lambda(T) = \begin{cases} 0 & T < T_s \\ \dfrac{T - T_s}{T_l - T_s} & T_s \le T \le T_l \\ 1 & T > T_l \end{cases}, \tag{5}$$

where T_s and T_l indicate solidus and liquidus temperatures, respectively.

A nonuniform mesh with 3.4 × 10^4 quadrilateral cells was used to discretise the computational domain, which according to our previous study [63] results in grid-independent predictions. For spatial discretisation and time integration, the second-order accurate QUICK scheme [64] and the first-order implicit scheme were applied, respectively. A constant time-step of 1 s was adopted in the simulations, following our previous study [63]. The PRESTO scheme [65] was employed for pressure interpolation, and the velocity-pressure coupling was achieved by the SIMPLE algorithm. The convergence criteria were set as 10^{-5}, 10^{-5}, and 10^{-7} for the scaled residuals of the mass, momentum, and energy equations, respectively. The validity of the present physics-based model in predicting the melting behaviour of phase-change material in a finned rectangular enclosure is demonstrated in our previous work [63]. The simulations were performed on a personal computer with an Intel Core i7 processor, employing six cores, and having a memory capacity of 16 GB.

Table 1
Thermophysical properties of Rubitherm RT82 and copper used in the simulations.

Property	Rubitherm RT82 [57, 58]	Copper [57]	Unit
Density ρ	950 (solid phase) 770 (liquid phase)	8978	kg m^{-3}
Specific heat capacity c_p	2000	381	J kg^{-1} K^{-1}
Thermal conductivity k	0.2	387.6	W m^{-1} K^{-1}
Dynamic viscosity μ	0.03499		Pa s
Latent heat of fusion H_f	176,000		J kg^{-1}
Solidus temperature T_s	351.15		K
Liquidus temperature T_l	355.15		K
Thermal expansion coefficient β	0.001		K^{-1}

Table 2
Summary of the cases studied using the physics-based computational model and the corresponding fin parameters.

Case ID	L_f [mm]	A_f [mm]	W_f [mm]	A_f/L_f [−]
F0 (straight fin)	20	0	2	0
F1	30	15	2	0.5
F2	30	10	2	0.333
F3	20	10	2	0.5
F4	40	5	3	0.125
F5	20	5	1	0.25
F6	30	10	3	0.333
F7	40	5	1	0.125
F8	40	10	2	0.25
F9	20	5	3	0.25
F10	20	15	1	0.75
F11	20	15	3	0.75
F12	40	15	3	0.375
F13	30	10	1	0.333
F14	30	5	2	0.166
F15	40	15	1	0.375

4. Data-driven model

Predicting the quantities of interest using the physics-based computational model can be computationally expensive and time-consuming and often requires high-performance computing facilities. To enhance the computational efficiency and reduce the computational cost of executing the physics-based numerical model, a feed-forward neural network (FFNN) is constructed to establish a relationship between the instantaneous liquid fraction, the energy stored in the system and the fin design parameters. An FFNN is a class of artificial neural network consisting of multiple layers of neurons connected by weighted

links, where each neuron performs a nonlinear transformation of its inputs and passes the output to the next layer [66]. The FFNN is used as a surrogate model to approximate the solution of the physics-based numerical model with much less computational resources.

The architecture of the fully connected multilayer perceptron (MLP) artificial neural network used in the present study is shown in Fig. 2, consisting of 4 input neurons, 4 hidden layers of 16 neurons each, and 2 output neurons. The input neurons represent the fin design parameters (*i.e.* length, thickness, and wave amplitude) and the flow time. The output neurons represent the energy stored in the system, which is related to the instantaneous liquid fraction and the mean temperature of the phase change material ($\overline{T}$) by an energy balance equation. The hidden layers are responsible for learning the complex nonlinear mapping between the inputs and the outputs. The artificial neural network used in the present work is implemented using MATLAB software. The FFNN is trained using a dataset generated by running the physics-based numerical model for different combinations of fin design parameters and measuring the corresponding energy stored in the system. The ADAM optimiser [67] was employed to increase the speed and stability of the learning process with learning rate of 0.001. The rectified linear unit (ReLU) activation function [66] is used. The trained FFNN was employed to predict the energy stored in the system for any given fin design parameters.

Approximately 1.2×10^5 data points were generated using the physics-based numerical simulations, which were partitioned into training (70% of data point), validation (15%), and testing (15%) subsets. The model acquires knowledge from the training dataset, which consists of input-output pairs that exemplify the desired behaviour of the model. The validation dataset aids in optimising hyperparameters, which are parameters that control the learning process and affect the model's complexity and performance. The testing dataset measures the model's performance on unseen data, which are data that are not used for training or validation. It is vital to separate these datasets to ensure that the model is both accurate, meaning that it minimises the error on the training data, and generalisable, meaning that it can perform well on new inputs that may differ from the training data. The data were normalised to the range [0, 1] using the minimum and maximum values to enhance the network accuracy and stability. The data points employed for training the neural network were selected through a random sampling process from the generated database. This random selection approach helps to ensure that the training dataset represents a diverse and unbiased subset of the entire dataset. Randomly selecting data points also reduces the potential for introducing systematic biases into the training process and contributes to the model's ability to generalize effectively to unseen data.

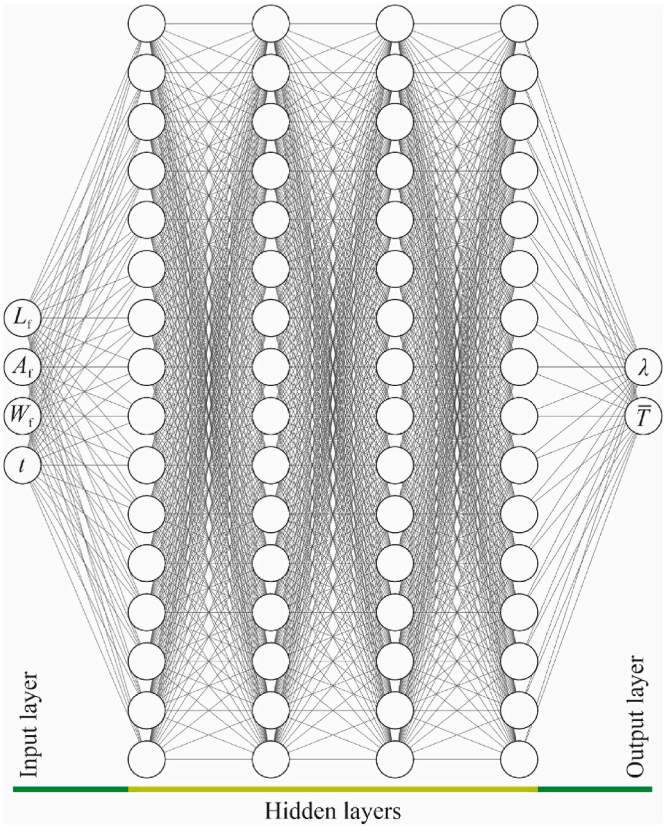

Fig. 2. The architecture of the fully connected multilayer perceptron (MLP) artificial neural network used in the present study with 4 input neurons, 4 hidden layers of 16 neurons, and 1 output neuron.

The accuracy of the neural network was assessed using three metrics: root mean square error (RMSE), mean absolute error (MAE), and correlation coefficient (R), which are given by:

$$\mathrm{RMSE} = \left(\sum_{i=1}^{N} \frac{(\widehat{y}_i - y_i)^2}{N} \right)^{\frac{1}{2}}, \tag{6}$$

$$\mathrm{MAE} = \sum_{i=1}^{N} \frac{|\widehat{y}_i - y_i|}{N}, \tag{7}$$

$$\mathrm{R} = \frac{1}{N-1} \sum_{i=1}^{N} \left(\frac{\widehat{y}_i - \widehat{\xi}}{\widehat{\sigma}} \right) \left(\frac{y_i - \xi}{\sigma} \right), \tag{8}$$

where N is the total number of data, y_i and $\widehat{y}_i$ are the predicted and ground truth values of the i-th data point respectively, ξ and $\widehat{\xi}$ are the mean deviation values of the predicted and ground truth data respectively, and σ and $\widehat{\sigma}$ are the standard deviation values of the predicted and ground truth data respectively.

5. Optimisation algorithm and procedure

To optimise the geometry of the fins, the particle swarm optimisation (PSO) technique [68] was employed, which is a metaheuristic technique that mimics the collective behaviour of swarms of animals or insects. The PSO algorithm operates on a population of potential solutions, called particles, that are randomly initialised and iteratively updated according to their own and the swarm's best positions in the search space. The objective function to be minimised or maximised by the PSO algorithm is called the fitness function. The PSO algorithm used in the present study is based on the algorithm proposed by Kennedy and Eberhart [69], with modifications suggested by Mezura-Montes and Coello [70] and Pedersen [71]. The main steps of the PSO algorithm are:

1. Initialise a swarm of particles with random positions and velocities in the search space.
2. Evaluate the fitness function for each particle.
3. Update the personal best position ($\mathscr{p}_{\mathrm{best}}$) for each particle as its current position if its fitness value is better than its previous personal best position.
4. Update the global best position ($\mathscr{g}_{\mathrm{best}}$) for the swarm as the position of the particle with the best fitness value among all global best positions.
5. Update the velocity and position of each particle using the following equations:

$$v_{i,j}^{(\ell+1)} = \omega v_{i,j}^{(\ell)} + c_1 r_1 \left(\mathscr{p}_{\mathrm{best}\,i,j} - x_{i,j}^{(\ell)} \right) + c_2 r_2 \left(\mathscr{g}_{\mathrm{best}\,j} - x_{i,j}^{(\ell)} \right), \tag{9}$$

$$x_{i,j}^{(\ell+1)} = x_{i,j}^{(\ell)} + v_{i,j}^{(\ell+1)}, \tag{10}$$

where $v_{i,j}^{(\ell)}$ and $x_{i,j}^{(\ell)}$ are the velocity and position of the j-th dimension

of the i-th particle at iteration $\mathscr{l}$, respectively; $\mathscr{w}$ is an inertia weight that controls the exploration and exploitation abilities of the swarm; $\mathscr{c}_1$ and $\mathscr{c}_2$ are acceleration coefficients that determine how much the particles are influenced by their own and the swarm's best positions; $\mathscr{r}_1$ and $\mathscr{r}_2$ are random numbers uniformly distributed in the range of [0, 1]; $\mathscr{p}_{\mathrm{best}ij}$ and $\mathscr{g}_{\mathrm{best}j}$ are the personal and global best positions of the j-th dimension, respectively.

6. Repeat steps 2 to 5 until a termination criterion is met, such as a maximum number of iterations or a maximum fitness value.

The PSO algorithm utilised in the present study was implemented using MATLAB. The PSO algorithm was applied to find the optimal values of length, height and thickness of the fins that maximise the average liquid fraction, hence the stored energy in the system, in 1 h. The search space was bounded by the ranges [20, 40 mm], [5, 15 mm] and [1, 3 mm] for length, wave amplitude, and thickness of the fins respectively. The fitness function was defined as:

$$\mathscr{f}\left(L_{\mathrm{f}}, A_{\mathrm{f}}, W_{\mathrm{f}}\right) = \frac{1}{3600}\int_0^{3600} \lambda(t)\mathrm{d}t, \tag{11}$$

where $\lambda(t)$ is the liquid fraction value at time t. To evaluate the fitness function for each particle at each iteration, the predictions obtained from the data-driven model were used. This way, running costly physics-based simulations was avoided for each particle, reducing the computational time of the optimisation process.

6. Results and discussion

6.1. Validation of the physics-based model

The validity of the physics-based model in predicting the solid-liquid phase transformation of PCM in LHTES systems was examined in our previous study [63]. In the present work, the numerical results obtained from the model are compared with numerical [36] and experimental data [72] reported in the literature, and the results are shown in Fig. 3. The problem involves melting of lauric acid in a rectangular enclosure equipped with three straight fins. The enclosure has a length of 120 mm and a height of 50 mm. The fins, made of aluminium, possess dimensions

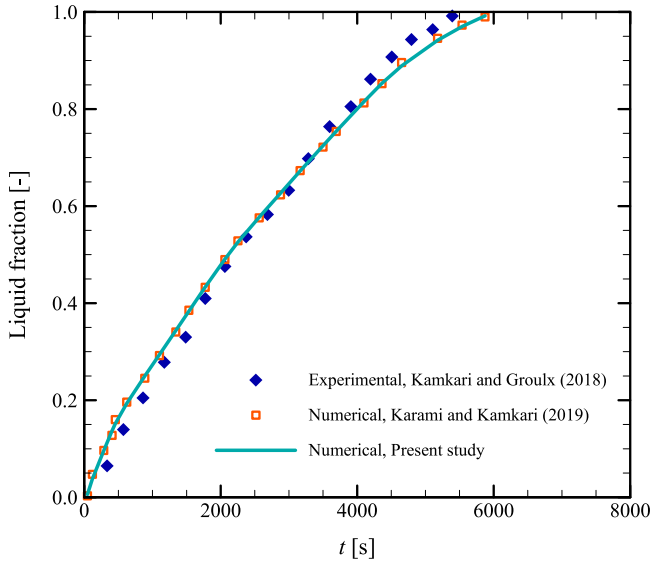

Fig. 3. Comparison of time evolution of the liquid fraction in a rectangular enclosure with three straight fins predicted by the present computational model (solid line) with available numerical [36] (squares) and experimental data [72] (diamonds).

of 4 mm in thickness, and 25 mm in length. The bottom wall of the enclosure is subjected to a constant temperature ($T_{\mathrm{w}} = 333.15$ K) to supply sufficient thermal energy to melt the material, while the remaining walls are thermally insulated. Additional information regarding the problem setup can be found in Refs. [36,72]. The time evolution of the liquid fraction in the enclosure, as predicted by the present model, demonstrates a satisfactory agreement with both the experimental and numerical data. The maximum absolute deviation between the predicted values and the experimental data is less than 6%. This indicates that the model accurately captures the phase transformation process and effectively reproduces the observed behaviour.

6.2. Results of the physics-based model

Fig. 4 shows the evolution of the temperature and velocity fields and the solid-liquid interface in the enclosure for the case with straight fins (F0) and cases with corrugated fins of different lengths (F2, F3 and F8). The addition of fins augments the effective heat transfer area and the depth of thermal penetration, accelerating the melting process in the enclosure. The effective heat transfer area is proportional to the fin length, which leads to a higher melting rate in the enclosure. As the melting advances, natural convection becomes more dominant in the energy transfer mechanism in the enclosure, resulting in a further enhancement of melting rate. Natural convection is driven by the buoyancy force due to the density difference between the hot and cold regions of the fluid. As more material melts, the buoyancy force becomes more significant compared to viscous forces, leading to stronger convection currents. Thermal plumes are buoyant jets of molten material that rise from the hot regions near the bottom wall and fins to the cold regions near the solid material, carrying thermal energy with them. When these plumes reach the solid-liquid interface, they transfer thermal energy to the solid material by convection, causing local melting and deformation of the interface. This results in the formation of a wavy solid-liquid interface that reflects the underlying flow structure. The predicted velocity field shows that the maximum velocity in the liquid region increases with time as more material melts, which is due to the intensification of natural convection in the enclosure. The maximum velocity in the enclosure with straight fins is similar to that in the enclosure with corrugated fins ($||\boldsymbol{V}||_{\mathrm{Max}} \approx 0.5 \pm 0.02$ mm s^{-1} at $t =$ 3600 s), but the corrugated fins induce more flow perturbations. These flow perturbations increase the mixing of hot and cold flows and heat transfer coefficients in the liquid region, improving the overall melting performance.

Fig. 5 presents the effect of fin length on the temporal variations of average liquid fraction and average temperature in the enclosure. A longer fin length enhances the melting rate and average temperature in the enclosure, thus increasing the amount of thermal energy stored in the system at a given time during charging. The results indicate that increasing the length of the corrugated fins increases the discharge rate. Moreover, the results show that employing corrugated fins improves the rate of energy extraction from the molten material compared to the case with straight fins.

Fig. 6 shows the effect of fin thickness (W_{f}) on the evolution of the temperature and velocity fields and the solid-liquid interface in the enclosure. The results suggest that employing thicker corrugated fins enhances the average velocity of the molten material in the enclosure. The predicted velocity field at $t = 3600$ s shows that the maximum velocity in the liquid region increases by about 34% (from 0.38 mm s^{-1} to 0.51 mm s^{-1}) when the fin thickness increases from 1 mm to 3 mm. This implies that the heat transfer coefficient between the fin and the liquid increases due to the intensification of natural convection, leading to a faster solid-liquid phase transformation in the enclosure. However, the fin thickness in the present problem has a negligible effect on the heat transfer surface area. Hence, the effect of fin thickness on the variations of average liquid fraction and average temperature in the enclosure seems insignificant, as shown in Fig. 7.

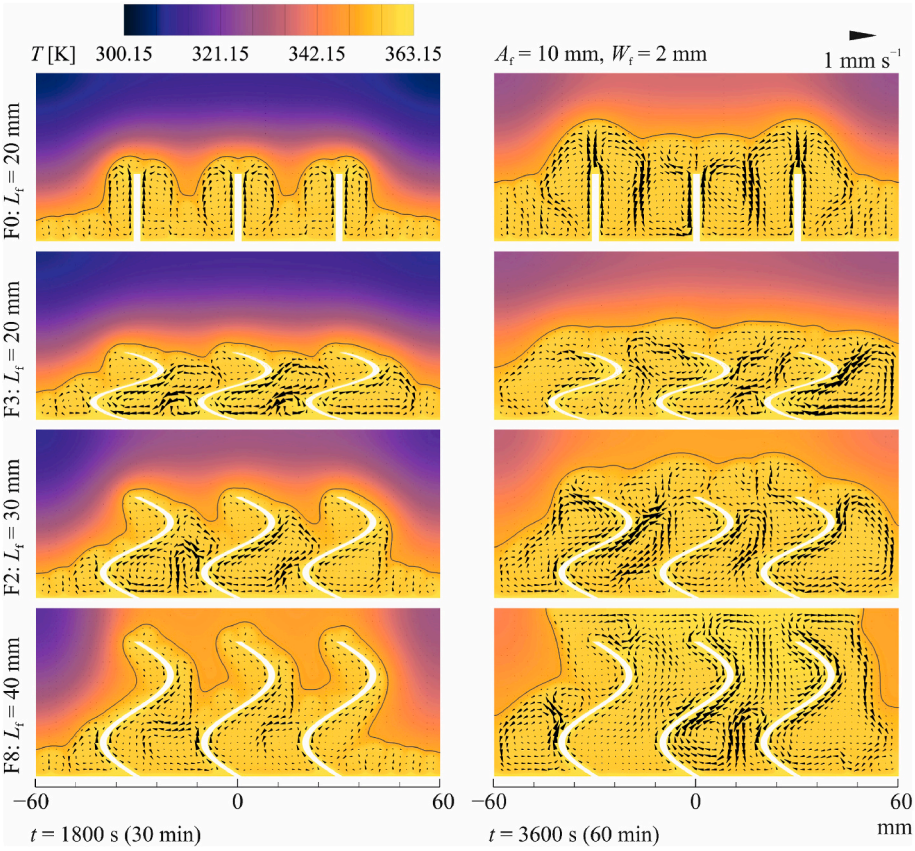

Fig. 4. Thermal and fluid flow fields in the enclosure for different fin lengths at $t = 1800$ s (left column) and $t = 3600$ s (right column). The solid-liquid interface is indicated by grey lines.

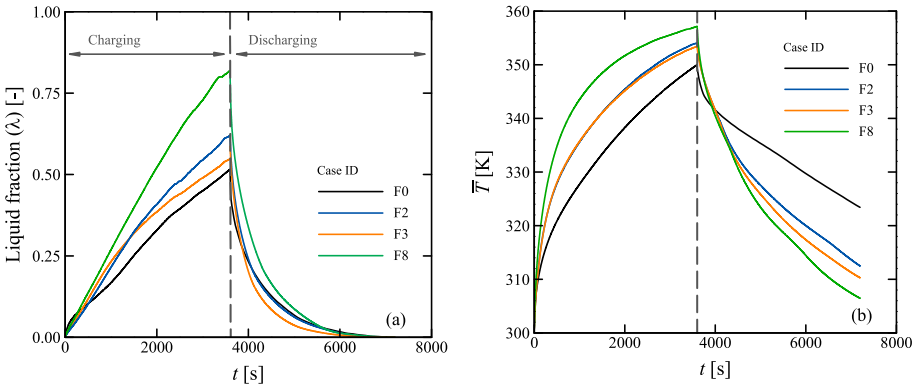

Fig. 5. Temporal variations of average liquid fraction (a) and average temperature (b) in the enclosure for different fin lengths.

Fig. 8 shows the effect of fin wave amplitude (A_f) on the evolution of the temperature and velocity fields and the solid-liquid interface in the enclosure. A larger fin wave amplitude increases the effective heat transfer surface area of the fin, which contributes to the improvement of the overall melting performance. However, a larger fin wave amplitude also disrupts the natural convection currents that transfer thermal energy from the hot surfaces to the solid material in the upper region of the enclosure. This is evident from the results shown in Fig. 8, which shows that the progress of the melting front in the enclosure slows down when A_f increases at any given time. The predicted velocity field at $t = 3600$ s indicates that the maximum velocity in the liquid region decreases by about 36% (from 0.57 mm s^{-1} to 0.42 mm s^{-1}) when A_f increases from 5 mm to 15 mm. These observations imply that the fin wave amplitude should be carefully designed to achieve the desired melting performance. Fig. 9 shows the effect of the fin wave amplitude on the temporal variations of average liquid fraction and average temperature in the enclosure. A more corrugated fin reduces the melting rate and average temperature in the enclosure, thus decreasing the amount of thermal energy stored in the system at a given time.

The thermal energy stored in the system consists of the latent and sensible heat of the phase change material (PCM) and the fins. Since the fins occupy less than 5% of the total volume of the system and have a much lower specific heat capacity than the PCM used (*i.e.* Rubitherm RT82), the thermal energy is mainly stored in the PCM. Therefore, incorporating properly designed fins in latent heat thermal energy storage systems can enhance their performance by increasing the heat transfer surface area and influencing the natural convection currents, despite reducing the PCM volume in the system. Neglecting the thermal

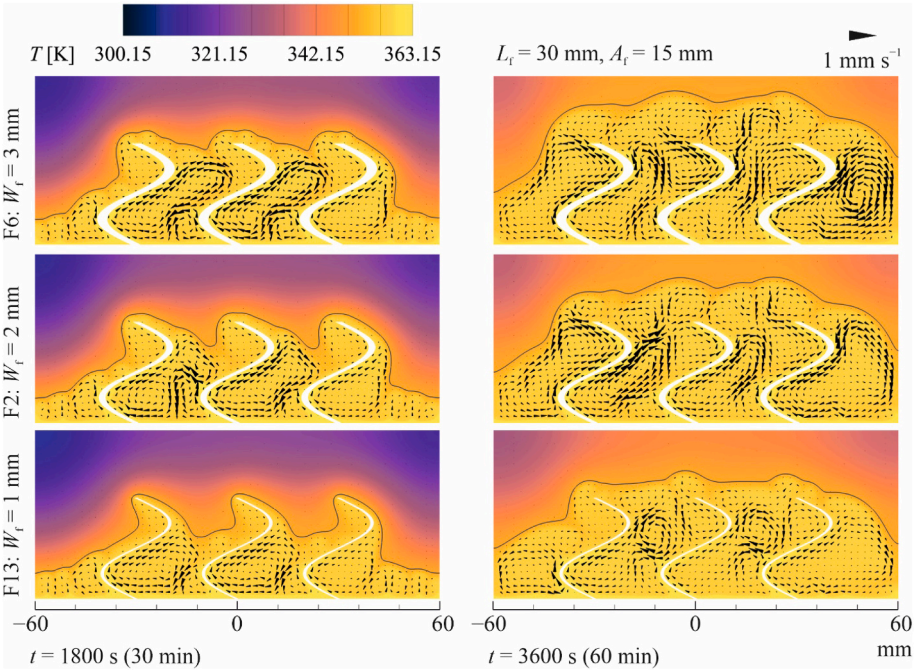

Fig. 6. Thermal and fluid flow fields in the enclosure for different fin thicknesses at $t = 1800$ s (left column) and $t = 3600$ s (right column). The solid-liquid interface is indicated by grey lines.

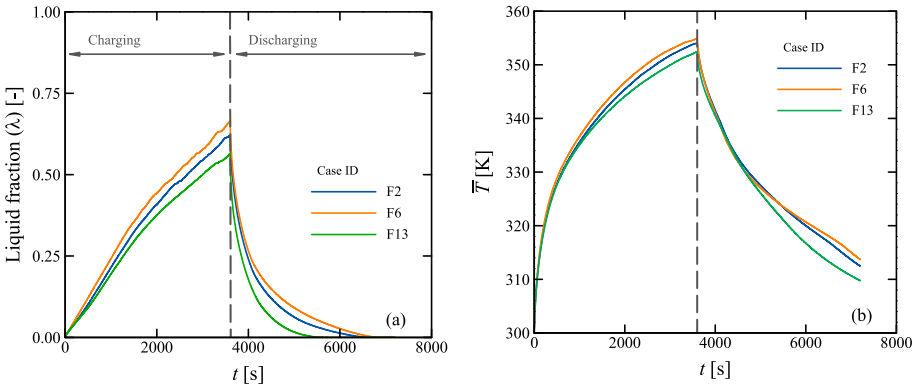

Fig. 7. Temporal variations of average liquid fraction (a) and average temperature (b) in the enclosure for different fin thicknesses.

energy stored in the fin, the thermal energy per unit mass stored in the system can be calculated as follows:

$$E_s = \lambda H_f + c_{pPCM} \bullet (\overline{T}_{PCM} - T_i), \quad (12)$$

where $\overline{T}$ is the average temperature, T_i is the initial temperature, and subscript 'PCM' indicates phase change material. Fig. 10 shows the dimensionless thermal energy per unit mass stored in the system at $t = 3600$ s for different cases, predicted by the physics-based model. The results show that the maximum amount of thermal energy is stored in cases F4 and F12, which have a fin length and thickness of 40 mm and 3 mm respectively but different fin wave amplitudes. Among all the cases simulated using the physics-based model, the case F10 ($L_f = 20$ mm, $A_f = 15$ mm, and $W_f = 1$ mm) has the lowest amount of stored thermal energy. The results demonstrate that the total thermal energy stored in the system is directly proportional to the volume of molten material in the system, which is represented by the liquid fraction λ.

6.3. Optimisation of the fin geometrical parameters using the data-driven model

The complexity and capacity of a neural network are determined by the number and size of its hidden layers. A neural network is composed of interconnected nodes that process and transmit information. Each node has a weight that represents its influence on the output of the network. During the learning process, these weights are adjusted to minimize a loss function, which quantifies the difference between the actual and desired outputs of the network. A feedforward neural network is a type of neural network that has no feedback loops, meaning that the information flows only in one direction, from the input layer to the output layer. The hidden layers are the intermediate layers between the input and output layers, where the nonlinear transformations of the data take place. The optimal number of hidden layers and neurons in each layer depends on the complexity of the problem solved by the neural network. The impact of the number of hidden layers and neurons on the performance metrics of the network was studied to identify the optimal neural network architecture for data-driven modelling. The performance metrics used in the present study are root mean square

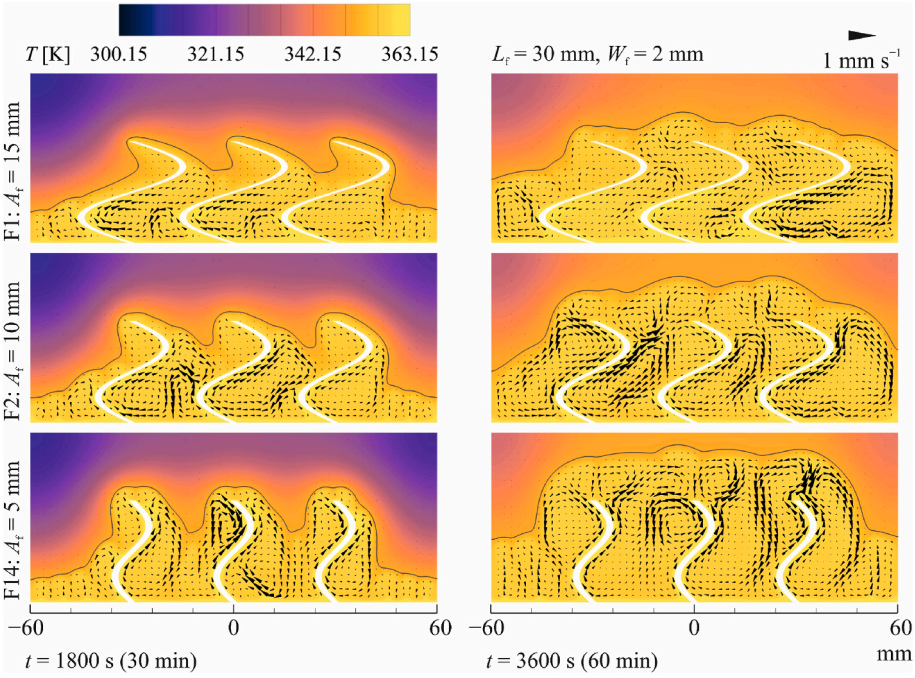

Fig. 8. Thermal and fluid flow fields in the enclosure for different fin wave amplitudes at $t = 1800$ s (left column) and $t = 3600$ s (right column). The solid-liquid interface is indicated by grey lines.

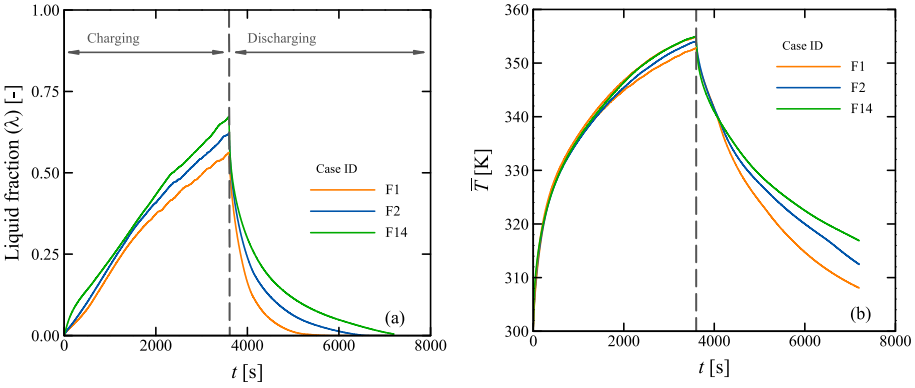

Fig. 9. Temporal variations of average liquid fraction (a) and average temperature (b) in the enclosure for different fin wave amplitudes.

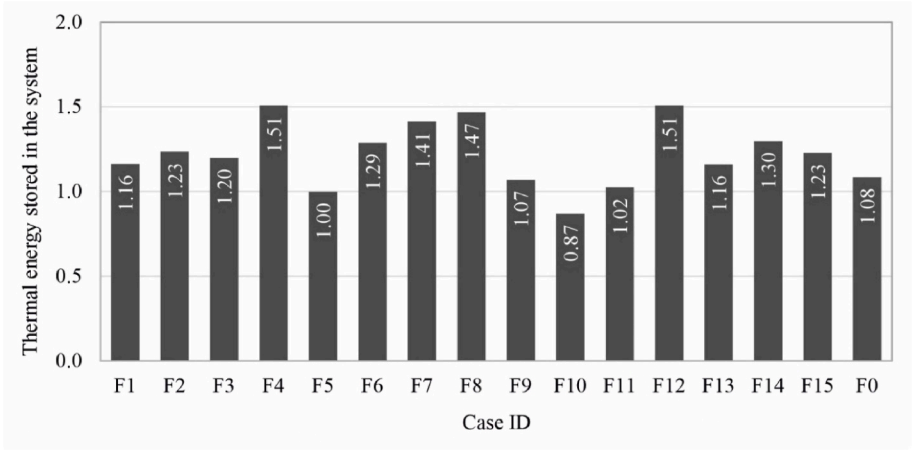

Fig. 10. Dimensionless thermal energy per unit mass stored in the system at $t = 3600$ s for different cases, predicted by the physics-based model. The thermal energy is normalised by the latent heat of fusion (H_f) of the phase change material.

error (RMSE), mean absolute error (MAE), and correlation coefficient (R). These metrics measure how well the network can predict the output values from the input values. Table 3 summarises the values of RMSE, MAE, and R for different combinations of hidden layers and neurons. Based on these results, a neural network that consists of 4 hidden layers with 16 neurons each was selected as the best architecture for the present problem.

The effect of the number of epochs of the learning process on the performance metrics (RMSE, MAE, and R) and the learning time is presented in Table 4. An epoch is a complete cycle of presenting all the training data to the neural network. The learning time is the duration of the learning process for a given number of epochs. The learning time increases almost linearly with increasing the number of epochs. Moreover, the values of RMSE and MAE decrease with increasing the number of epochs. For epoch values less than 200, the value of RMSE and MAE decreases significantly with an increase in the number of epochs, indicating improvement in the neural network performance. For epoch values greater than 200, changes in the value of RMSE and MAE are insignificant, indicating that the neural network has reached its optimal performance. In other words, choosing an epoch number greater than 200 increased the computational cost without significantly increasing the accuracy of the neural network. Therefore, an epoch number of 200 was selected as the appropriate number for the learning process.

The predicted liquid fraction (λ) and dimensionless average temperature (T^*) from the data-driven model were compared with the corresponding values from the physics-based model, as shown in Fig. 11. The results showed a good agreement between the two models, with a maximum deviation of less than 8%. The deviation was calculated as the absolute difference between the data-driven model prediction and the physics-based model prediction divided by the physics-based model prediction. The data-driven model can reproduce the physics-based model predictions with reasonable accuracy, as evidenced by the low deviation values and the close alignment of the data points along the 45-degree line. The data-driven model is also able to capture the main trends and features of the phase change process and the thermal behaviour of the system, as explained by the physics-based model.

The PSO algorithm was employed with two swarm sizes (30 and 100) to determine the optimal values of length L_f, wave amplitude A_f, and thickness W_f for the fins in a latent thermal energy storage system. The optimal values obtained by the PSO algorithm for each swarm size are: [L_f: 40.000 mm, A_f: 11.345 mm, W_f: 3.000 mm] and [40.000, 11.344, 3.000 mm] respectively. These values are very close to each other, indicating the robustness and consistency of the PSO algorithm. Physics-based numerical simulations were conducted to validate the predicted liquid fraction values by the data-driven model for the optimal geometry values. The predicted thermal and fluid flow fields in the enclosure with the optimised fin geometry are shown in Fig. 12. The average liquid fraction in the enclosure over a period of 1 h charging for the optimal fin geometry ([L_f, A_f, W_f] = [40.000, 11.344, 3.000 mm]) is 0.527 (predicted using the data-driven model) and 0.523 (predicted using the physics-based model), with a difference of less than 1%, confirming the accuracy and reliability of the data-driven model. The maximum velocity in the liquid region at t = 3600 s is about 0.67 mm s^{-1}. The optimal fin geometry resulted in a liquid fraction of 0.88 and an average temperature of 358.85 K at t = 3600 s, which corresponds to a dimensionless thermal energy per unit mass stored in the system (E_s/H_f) equal to 1.55. This surpasses all other geometries tested in the study, as reported in Fig. 10.

The effect of each geometrical parameter of the fin on the liquid fraction in the thermal energy storage system was studied using the data-driven model. Three graphs were generated to depict this relationship, as presented in Fig. 13, showing the predicted liquid fraction at t = 3600 s as a function of two geometrical parameters: length, height, or thickness. In each graph, one of the geometrical parameters is set to its optimal value obtained from the PSO algorithm, while the other two parameters are varied within their respective ranges. These graphs provide insights into how the liquid fraction changes with different combinations of geometrical parameters. Furthermore, they prominently showcase the optimal point derived from the PSO algorithm, representing the combination of parameters that result in the highest liquid fraction and the thermal energy stored in the system.

7. Conclusions

This study aimed at optimising fin geometry for enhancing melting performance in latent heat thermal energy storage (LHTES) systems. A combined approach of physics-based modelling and data-driven optimisation was employed to analyse the solid-liquid phase transformation of a phase change material (PCM) in an enclosure equipped with corrugated fins.

The physics-based model was validated by comparing numerical results with experimental and numerical data from the literature. The results showed a satisfactory agreement between the model predictions and the data, demonstrating the accuracy of the model in capturing the phase transformation process. The results of the physics-based model show that the addition of fins results in increased effective heat transfer area and depth of thermal penetration, accelerating the melting process. Natural convection is found to play a significant role in enhancing the mixing of hot and cold flows and heat transfer coefficients in the liquid region.

The effects of different fin geometries, namely straight fins and corrugated fins, on the performance of the LHTES system were compared. It was found that corrugated fins induced more flow perturbations than straight fins, thereby improving overall melting

Table 3
The effect of the number of hidden layers and the number of neurons on the accuracy of the predictions.

Hidden Layers				No. Weights	RMSE			MAE			R		
1st	2nd	3rd	4th		Training	Validation	Testing	Training	Validation	Testing	Training	Validation	Testing
16	0	0	0	97	4.13E-02	4.15E-02	4.14E-02	3.27E-02	3.28E-02	3.29E-02	0.990427	0.990303	0.990348
32	0	0	0	193	4.52E-02	4.57E-02	4.55E-02	3.44E-02	3.46E-02	3.46E-02	0.034578	0.034578	0.988311
64	0	0	0	385	3.01E-02	3.02E-02	3.02E-02	2.31E-02	2.31E-02	2.32E-02	0.994926	0.994885	0.994899
128	0	0	0	769	2.78E-02	2.78E-02	2.79E-02	2.25E-02	2.25E-02	2.27E-02	0.995680	0.995664	0.995642
16	16	0	0	369	3.25E-02	3.26E-02	3.27E-02	2.41E-02	2.41E-02	2.43E-02	0.994057	0.994033	0.993984
32	32	0	0	1249	2.07E-02	2.06E-02	2.09E-02	1.50E-02	1.49E-02	1.52E-02	0.997602	0.997638	0.997569
64	64	0	0	4545	1.89E-02	1.90E-02	1.89E-02	1.41E-02	1.42E-02	1.41E-02	0.998003	0.997975	0.998002
128	128	0	0	17,281	1.18E-02	1.18E-02	1.18E-02	8.88E-03	8.89E-03	8.93E-03	0.999233	0.999230	0.999228
16	32	16	0	1169	1.39E-02	1.39E-02	1.39E-02	1.06E-02	1.06E-02	1.06E-02	0.998923	0.998916	0.998917
32	64	32	0	4385	1.27E-02	1.28E-02	1.27E-02	9.38E-03	9.43E-03	9.43E-03	0.999115	0.999104	0.999113
64	128	64	0	16,961	1.02E-02	1.02E-02	1.02E-02	7.78E-03	7.78E-03	7.84E-03	0.999426	0.999422	0.999419
128	128	128	0	33,793	1.03E-02	1.04E-02	1.03E-02	7.90E-03	7.94E-03	7.94E-03	0.999410	0.999403	0.999408
16	16	16	16	913	1.47E-02	1.48E-02	1.48E-02	1.11E-02	1.11E-02	1.11E-02	0.998788	0.998780	0.998778
16	64	64	16	6385	1.34E-02	1.34E-02	1.34E-02	9.91E-03	9.93E-03	9.98E-03	0.999010	0.999006	0.998999
64	128	128	64	33,473	9.92E-03	9.97E-03	9.96E-03	7.53E-03	7.56E-03	7.58E-03	0.999456	0.999450	0.999451

Table 4
The effect of the number of epochs on the learning process.

Epoch	Learning Time [s]	RMSE			MAE			R		
		Training	Validation	Testing	Training	Validation	Testing	Training	Validation	Testing
5	1.00	2.74E-01	2.75E-01	2.74E-01	2.25E-01	2.26E-01	2.25E-01	0.424947	0.419205	0.419331
10	2.00	1.71E-01	1.70E-01	1.71E-01	1.40E-01	1.40E-01	1.41E-01	0.884606	0.884884	0.881611
20	5.00	5.85E-02	5.88E-02	5.84E-02	4.67E-02	4.70E-02	4.68E-02	0.980675	0.980523	0.980683
50	11.00	3.46E-02	3.48E-02	3.46E-02	2.79E-02	2.82E-02	2.80E-02	0.993293	0.993187	0.993259
100	26.00	1.47E-02	1.48E-02	1.48E-02	1.11E-02	1.11E-02	1.11E-02	0.998788	0.998780	0.998778
200	54.00	1.16E-02	1.16E-02	1.16E-02	8.71E-03	8.67E-03	8.71E-03	0.999255	0.999258	0.999252
500	138.00	1.09E-02	1.09E-02	1.09E-02	8.12E-03	8.07E-03	8.15E-03	0.999332	0.999337	0.999329

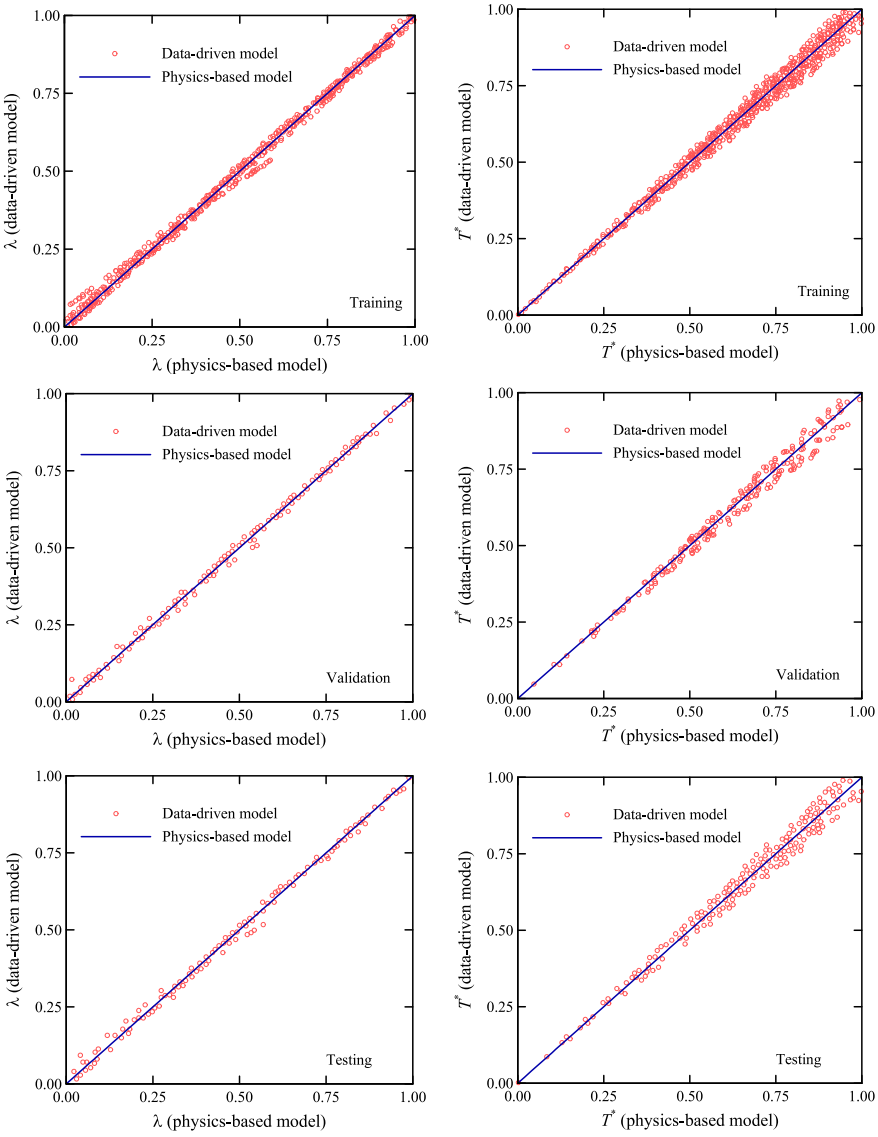

Fig. 11. Comparison of predicted liquid fraction and dimensionless average temperature in the enclosure from the data-driven model (symbols) with the corresponding values from the physics-based model (solid line). The top row shows the results for the training batch, the middle row shows the results for the validation batch and the bottom row shows the results for the testing batch.

performance. However, larger fin wave amplitudes slowed down the progress of the melting front by disrupting natural convection currents. Thus, a careful balance between increasing heat transfer surface area and maintaining effective natural convection was highlighted.

The influence of fin length, thickness, and wave amplitude on the temporal variations of average liquid fraction and average temperature was also explored. It was observed that longer fin lengths and thicker fins enhanced the melting rate and average temperature, increasing the amount of thermal energy stored in the system during charging. However, the effect of fin thickness on thermal characteristics was relatively insignificant. These findings provide valuable guidelines for optimising fin geometry in LHTES systems. By incorporating appropriately designed fins, the performance of such systems can be significantly enhanced, despite the reduction in PCM volume.

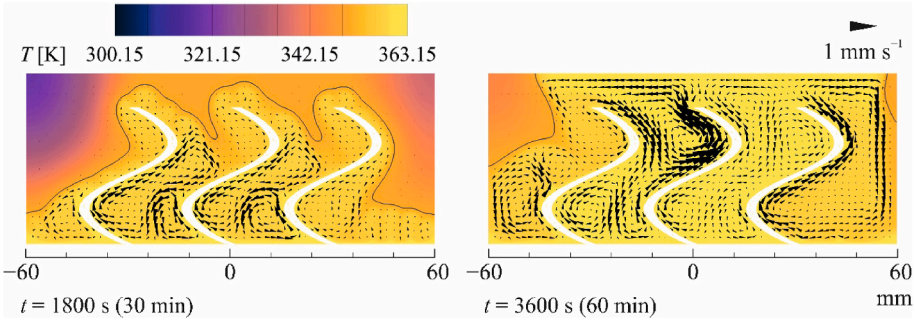

Fig. 12. Thermal and fluid flow fields in the enclosure equipped with the optimised fin geometry at $t = 1800$ s (left column) and $t = 3600$ s (right column). The solid-liquid interface is indicated by grey lines.

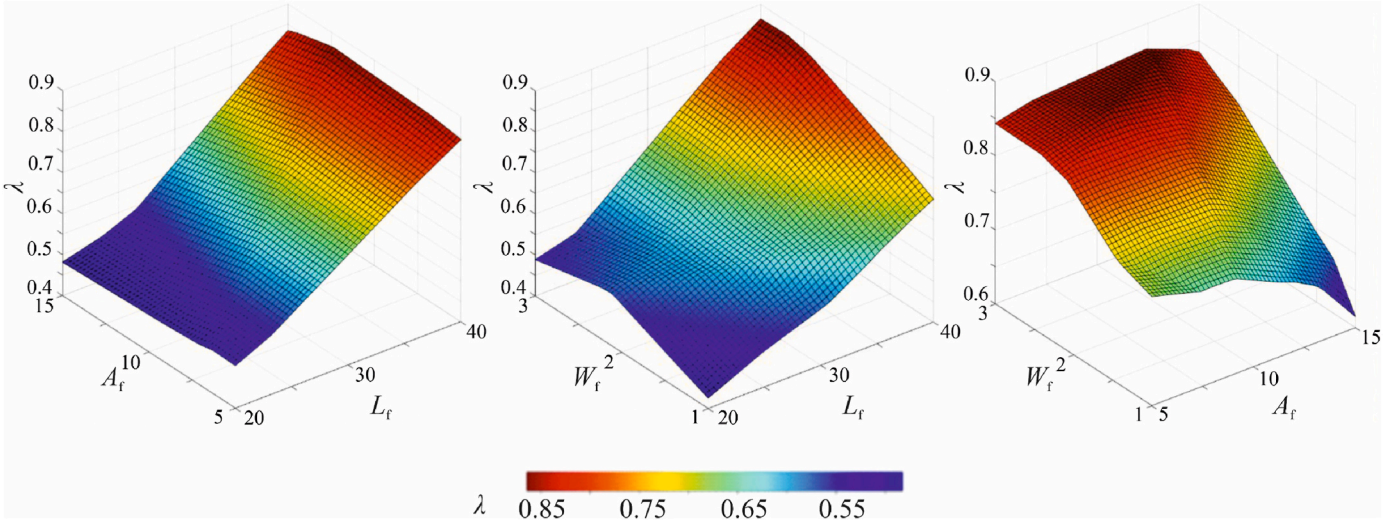

Fig. 13. The effect of different geometrical parameters of the fin on the liquid fraction in the thermal energy storage system at $t = 3600$ s. The data were generated using the data-driven model.

Furthermore, a data-driven model based on a neural network in conjunction with the particle swarm optimisation was employed to optimise fin geometry. The best-performing network configuration consisted of four hidden layers with 16 neurons each, as identified through analysis of various network architectures. The data-driven model was able to reproduce the physics-based model predictions with high accuracy and was used to find the optimal fin geometry that maximised the dimensionless thermal energy per unit mass stored in the system.

Future research can expand upon these findings by exploring various fin geometries, investigating the effects of different PCM, and considering the impact of external factors such as varying ambient conditions. Furthermore, expanding the study to other types of thermal energy systems and exploring novel materials for PCM can further advance the field of thermal energy storage and contribute to sustainable energy utilisation.

CRediT authorship contribution statement

Ali Tavakoli: Conceptualization, Methodology, Software, Validation, Formal analysis, Investigation, Data curation, Writing – original draft, Writing – review & editing, Visualization. **Javad Hashemi:** Visualization, Methodology, Investigation, Formal analysis, Writing – review & editing. **Mahyar Najafian:** Software, Formal analysis. **Amin Ebrahimi:** Conceptualization, Methodology, Validation, Formal analysis, Visualization, Supervision, Project administration, Investigation, Resources, Writing - original draft, Writing - review & editing.

Declaration of competing interest

The authors declare that they have no known competing financial interests or personal relationships that could have appeared to influence the work reported in this paper.

Data availability

Data will be made available on request.

Appendix

Figure A1 shows the computational grid used in the physics-based numerical simulations.

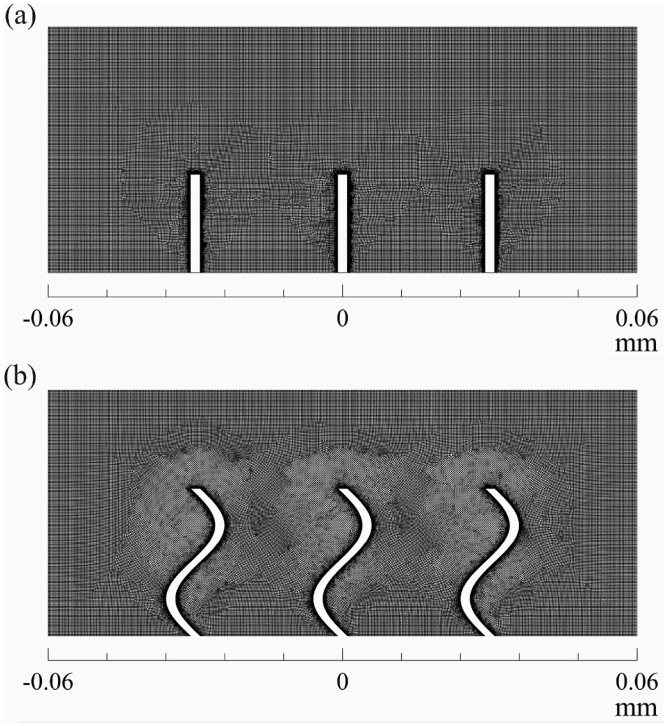

Fig. A1. The computational grid used in the simulations for (a) Case F0, and (b) Case F14.

References

[1] I. Sarbu, C. Sebarchievici, A comprehensive review of thermal energy storage, Sustainability 10 (1) (2018) 191, https://doi.org/10.3390/su10010191.

[2] G. Alva, Y. Lin, G. Fang, An overview of thermal energy storage systems, Energy 144 (2018) 341–378, https://doi.org/10.1016/j.energy.2017.12.037.

[3] A. Sharma, et al., Review on thermal energy storage with phase change materials and applications, Renew. Sustain. Energy Rev. 13 (2) (2009) 318–345, https://doi.org/10.1016/j.rser.2007.10.005.

[4] K. Pielichowska, K. Pielichowski, Phase change materials for thermal energy storage, Prog. Mater. Sci. 65 (2014) 67–123, https://doi.org/10.1016/j.pmatsci.2014.03.005.

[5] X. Zhang, et al., Mechanism study on the synergistic coupling of the double-dish solar latent heat storage system to enhance heat transfer, Energy Rep. 9 (2023) 730–741, https://doi.org/10.1016/j.egyr.2022.12.028.

[6] A. Sharma, R. Pitchumani, R. Chauhan, Melting and solidification performance investigation of latent heat storage unit designs for low-temperature solar thermal applications, J. Energy Storage 66 (2023), 107323, https://doi.org/10.1016/j.est.2023.107323.

[7] B. Lamrani, et al., Dynamic thermal analysis of a coupled solar water heaters-thermal storage tank for solar powered district heating networks, J. Energy Storage 61 (2023), 106793, https://doi.org/10.1016/j.est.2023.106793.

[8] M.A. Pans, G. Claudio, P.C. Eames, Modelling of 4th generation district heating systems integrated with different thermal energy storage technologies - methodology, Energy Convers. Manag. 276 (2023), 116545, https://doi.org/10.1016/j.enconman.2022.116545.

[9] L.A. de Araujo Passos, et al., Dynamic optimization for minimal hvac demand with latent heat storage, heat recovery, natural ventilation, and solar shadings, Energy Convers. Manag. 276 (2023), 116573, https://doi.org/10.1016/j.enconman.2022.116573.

[10] M. Mohkam, et al., Impacts of phase change materials on performance of operational peak load shifting strategies in a sample building in hot-arid climate, Environ. Prog. Sustain. Energy 42 (1) (2023), e13961, https://doi.org/10.1002/ep.13961.

[11] Z. Sun, et al., Experimental study of battery passive thermal management system using copper foam-based phase change materials, Int. J. Thermofluids 17 (2023), 100255, https://doi.org/10.1016/j.ijft.2022.100255.

[12] R. Huang, et al., Experimental and numerical study of pcm thermophysical parameters on lithium-ion battery thermal management, Energy Rep. 6 (2020) 8–19, https://doi.org/10.1016/j.egyr.2019.09.060.

[13] L. Jesús, et al., Advances in thermal energy storage materials and their applications towards zero energy buildings: a critical review, Appl. Energy 203 (2017) 219–239, https://doi.org/10.1016/j.apenergy.2017.06.008.

[14] M.H. Zahir, et al., Challenges of the application of PCMs to achieve zero energy buildings under hot weather conditions: a review, J. Energy Storage 64 (2023), 107156, https://doi.org/10.1016/j.est.2023.107156.

[15] M. Liu, et al., Review of research progress on corrosion and anti-corrosion of phase change materials in thermal energy storage systems, J. Energy Storage 63 (2023), 107005, https://doi.org/10.1016/j.est.2023.107005.

[16] O.M. Adesusi, et al., A comprehensive review of the materials degradation phenomena in solid-liquid phase change materials for thermal energy storage, Int. J. Thermofluids 18 (2023), 100360, https://doi.org/10.1016/j.ijft.2023.100360.

[17] Z. Li, et al., Applications and technological challenges for heat recovery, storage and utilisation with latent thermal energy storage, Appl. Energy 283 (2021), 116277, https://doi.org/10.1016/j.apenergy.2020.116277.

[18] K. Tofani, S. Tiari, Nano-enhanced phase change materials in latent heat thermal energy storage systems: a review, Energies 14 (2021) 3821, https://doi.org/10.3390/en14133821.

[19] M. Ghalambaz, et al., Melting process of the nano-enhanced phase change material (nepcm) in an optimized design of shell and tube thermal energy storage (TES): taguchi optimization approach, Appl. Therm. Eng. 193 (2021), 116945, https://doi.org/10.1016/j.applthermaleng.2021.116945.

[20] M. Mahdavi, S. Tiari, V. Pawar, A numerical study on the combined effect of dispersed nanoparticles and embedded heat pipes on melting and solidification of a shell and tube latent heat thermal energy storage system, J. Energy Storage 27 (2020), 101086, https://doi.org/10.1016/j.est.2019.101086.

[21] L. Bo, et al., Twisted-fin parametric study to enhance the solidification performance of phase-change material in a shell-and-tube latent heat thermal energy storage system, J. Comput. Des. Eng. 9 (6) (2021) 2297–2313, https://doi.org/10.1093/jcde/qwac107.

[22] K. Shank, et al., Experimental study of varying heat transfer fluid parameters within a latent heat thermal energy storage system enhanced by fins, Sustainability 14 (2022) 8920, https://doi.org/10.3390/su14148920.

[23] S.A.M. Mehryan, et al., Optimum configuration of a metal foam layer for a fast thermal charging energy storage unit: a numerical study, J. Energy Storage 48 (2022), 103950, https://doi.org/10.1016/j.est.2021.103950.

[24] W. Cui, et al., Heat transfer analysis of phase change material composited with metal foam-fin hybrid structure in inclination container by numerical simulation and artificial neural network, Energy Rep. 8 (2022) 10203–10218, https://doi.org/10.1016/j.egyr.2022.07.178.

[25] R. Qaiser, et al., Performance enhancement of latent energy storage system using effective designs of tubes and shell, Energy Rep. 8 (2022) 3856–3872, https://doi.org/10.1016/j.egyr.2022.03.028.

[26] W. Ye, D. Jamshideasli, J.M. Khodadadi, Improved performance of latent heat energy storage systems in response to utilization of high thermal conductivity, Fins 16 (3) (2023) 1277, https://doi.org/10.3390/en16031277.

[27] S. Sami, N. Etesami, Heat transfer enhancement of microencapsulated phase change material by addition of nanoparticles for a latent heat thermal energy

storage system, Energy Rep. 7 (2021) 4930–4940, https://doi.org/10.1016/j.egyr.2021.07.080.
[28] A. Kumar, S.K. Saha, Performance analysis of a packed bed latent heat thermal energy storage with cylindrical-shaped encapsulation, Int. J. Energy Res. 45 (9) (2021) 13130–13148, https://doi.org/10.1002/er.6639.
[29] T. Xu, et al., Experimental and numerical investigation of a latent heat thermal energy storage unit with ellipsoidal macro-encapsulation, Energy 238 (2022), 121828, https://doi.org/10.1016/j.energy.2021.121828.
[30] S. Zhang, S. Mancin, L. Pu, A review and prospective of fin design to improve heat transfer performance of latent thermal energy storage, J. Energy Storage 62 (2023), 106825, https://doi.org/10.1016/j.est.2023.106825.
[31] N. Modi, X. Wang, M. Negnevitsky, Experimental investigation of the effects of inclination, fin height, and perforation on the thermal performance of a longitudinal finned latent heat thermal energy storage, Energy 274 (2023), 127327, https://doi.org/10.1016/j.energy.2023.127327.
[32] L. Wang, et al., Performance enhancement of a horizontal latent thermal energy storage unit with elliptical fins, Appl. Therm. Eng. 225 (2023), 120191, https://doi.org/10.1016/j.applthermaleng.2023.120191.
[33] L. Darvishvand, et al., Machine learning-based prediction of transient latent heat thermal storage in finned enclosures using group method of data handling approach: a numerical simulation, Eng. Anal. Bound. Elem. 143 (2022) 61–77, https://doi.org/10.1016/j.enganabound.2022.06.009.
[34] Y. Tian, et al., Bionic topology optimization of fins for rapid latent heat thermal energy storage, Appl. Therm. Eng. 194 (2021), 117104, https://doi.org/10.1016/j.applthermaleng.2021.117104.
[35] S. Tiari, A. Hockins, K. Shank, Experimental study of a latent heat thermal energy storage system assisted by varying annular fins, J. Energy Storage 55 (2022), 105603, https://doi.org/10.1016/j.est.2022.105603.
[36] R. Karami, B. Kamkari, Investigation of the effect of inclination angle on the melting enhancement of phase change material in finned latent heat thermal storage units, Appl. Therm. Eng. 146 (2019) 45–60, https://doi.org/10.1016/j.applthermaleng.2018.09.105.
[37] S.-B. Chen, et al., Combined effect of using porous media and nano-particle on melting performance of pcm filled enclosure with triangular double fins, Case Stud. Therm. Eng. 25 (2021), 100939, https://doi.org/10.1016/j.csite.2021.100939.
[38] J. Li, et al., Effect of twisted fins on the melting performance of pcm in a latent heat thermal energy storage system in vertical and horizontal orientations: energy and exergy analysis, Appl. Therm. Eng. 219 (2023), 119489, https://doi.org/10.1016/j.applthermaleng.2022.119489.
[39] M. Eslami, F. Khosravi, H.R. Fallah Kohan, Effects of fin parameters on performance of latent heat thermal energy storage systems: a comprehensive review, Sustain. Energy Technol. Assessments 47 (2021), 101449, https://doi.org/10.1016/j.seta.2021.101449.
[40] J. Pássaro, et al., Effect of fins and nanoparticles in the discharge performance of pcm thermal storage system with a multi pass finned tube heat exchange, Appl. Therm. Eng. 212 (2022), 118569, https://doi.org/10.1016/j.applthermaleng.2022.118569.
[41] V. Safari, H. Abolghasemi, B. Kamkari, Experimental and numerical investigations of thermal performance enhancement in a latent heat storage heat exchanger using bifurcated and straight fins, Renew. Energy 174 (2021) 102–121, https://doi.org/10.1016/j.renene.2021.04.076.
[42] H.M. Ali, A. Arshad, Experimental investigation of N-eicosane based circular pin-fin heat sinks for passive cooling of electronic devices, Int. J. Heat Mass Tran. 112 (2017) 649–661, https://doi.org/10.1016/j.ijheatmasstransfer.2017.05.004.
[43] P. Srivatsa, R. Baby, C. Balaji, Geometric optimization of a PCM-based heat sink—a coupled ANN and GA approach, Heat Tran. Eng. 37 (10) (2016) 875–888, https://doi.org/10.1080/01457632.2015.1089749.
[44] S. Baghaei Oskouei, Ö. Bayer, Experimental and numerical investigation of melting and solidification enhancement using fibonacci-inspired fins in a latent thermal energy storage unit, Int. J. Heat Mass Tran. 210 (2023), 124180, https://doi.org/10.1016/j.ijheatmasstransfer.2023.124180.
[45] S. Jiang, Y. Huang, Investigation on the heat discharge performance of a bioinspired latent heat exchanger with leaf-like fins, Sustain. Energy Technol. Assessments 57 (2023), 103187, https://doi.org/10.1016/j.seta.2023.103187.
[46] J. Jiang, et al., Numerical analysis on heat transfer and melting characteristics of a solid-liquid phase change process in a rectangular cavity inserted with bifurcated fractal fins, Int. Commun. Heat Mass Tran. 142 (2023), 106616, https://doi.org/10.1016/j.icheatmasstransfer.2023.106616.
[47] P. Yan, et al., Performance enhancement of phase change materials in triplex-tube latent heat energy storage system using novel fin configurations, Appl. Energy 327 (2022), 120064, https://doi.org/10.1016/j.apenergy.2022.120064.
[48] F. Jiao, et al., Numerical investigation on melting and thermal performances of a phase change material in partitioned cavities with fins for thermal energy storage, J. Energy Storage 56 (2022), 106022, https://doi.org/10.1016/j.est.2022.106022.
[49] I.A. Laasri, et al., Investigation of different topology-optimized fin structures in a cylindrical latent heat thermal energy storage unit, Therm. Sci. Eng. Prog. 33 (2022), 101372, https://doi.org/10.1016/j.tsep.2022.101372.
[50] A.-C. Iradukunda, et al., Transient thermal performance using phase change material integrated topology optimized heat sinks, Appl. Therm. Eng. 179 (2020), 115723, https://doi.org/10.1016/j.applthermaleng.2020.115723.
[51] R. Ge, et al., Additive manufacturing of a topology-optimised multi-tube energy storage device: experimental tests and numerical analysis, Appl. Therm. Eng. 180 (2020), 115878, https://doi.org/10.1016/j.applthermaleng.2020.115878.
[52] C. Deng, et al., Self-directed online machine learning for topology optimization, Nat. Commun. 13 (1) (2022) 388, https://doi.org/10.1038/s41467-021-27713-7.
[53] X. Wang, Y. Zhao, F. Pourpanah, Recent advances in deep learning, International Journal of Machine Learning and Cybernetics 11 (4) (2020) 747–750, https://doi.org/10.1007/s13042-020-01096-5.
[54] Y. LeCun, Y. Bengio, G. Hinton, Deep learning, Nature 521 (7553) (2015) 436–444, https://doi.org/10.1038/nature14539.
[55] K. Ermis, A. Erek, I. Dincer, Heat transfer analysis of phase change process in a finned-tube thermal energy storage system using artificial neural network, Int. J. Heat Mass Tran. 50 (15–16) (2007) 3163–3175, https://doi.org/10.1016/j.ijheatmasstransfer.2006.12.017.
[56] S. Motahar, Experimental study and ann-based prediction of melting heat transfer in a uniform heat flux pcm enclosure, J. Energy Storage 30 (2020), 101535, https://doi.org/10.1016/j.est.2020.101535.
[57] S. Mat, et al., Enhance heat transfer for pcm melting in triplex tube with internal-external fins, Energy Convers. Manag. 74 (2013) 223–236, https://doi.org/10.1016/j.enconman.2013.05.003.
[58] F. Li, et al., Application and analysis of flip mechanism in the melting process of a triplex-tube latent heat energy storage unit, Energy Rep. 9 (2023) 3989–4004, https://doi.org/10.1016/j.egyr.2023.03.037.
[59] D.J. Tritton, Physical Fluid Dynamics, second ed., Clarendon Press (Oxford science publications, Oxford England, 1988.
[60] V.R. Voller, C. Prakash, A fixed grid numerical modelling methodology for convection-diffusion mushy region phase-change problems, Int. J. Heat Mass Tran. 30 (8) (1987) 1709–1719, https://doi.org/10.1016/0017-9310(87)90317-6.
[61] A. Ebrahimi, C.R. Kleijn, I.M. Richardson, Sensitivity of numerical predictions to the permeability coefficient in simulations of melting and solidification using the enthalpy-porosity method, Energies 12 (22) (2019) 4360, https://doi.org/10.3390/en12224360.
[62] V.R. Voller, C.R. Swaminathan, General source-based method for solidification phase change, Numer. Heat Tran., Part B: Fundamentals 19 (1990) 175–189, https://doi.org/10.1080/10407799108944962.
[63] A. Tavakoli, M. Farzaneh-Gord, A. Ebrahimi-Moghadam, Using internal sinusoidal fins and phase change material for performance enhancement of thermal energy storage systems: heat transfer and entropy generation analyses, Renew. Energy 205 (2023) 222–237, https://doi.org/10.1016/j.renene.2023.01.074.
[64] B.P. Leonard, S. Mokhtari, ULTRA-SHARP Nonoscillatory Convection Schemes for High-Speed Steady Multidimensional Flow, 1990 (No. ICOMP-90-12).
[65] C.-J. Hsu, Numerical heat transfer and fluid flow, Nucl. Sci. Eng. 78 (2) (1981) 196–197, https://doi.org/10.13182/NSE81-A20112.
[66] J. Schmidhuber, Deep learning in neural networks: an overview, Neural Network. 61 (2015) 85–117, https://doi.org/10.1016/j.neunet.2014.09.003.
[67] D.P. Kingma, J. Ba, Adam: a method for stochastic optimization. http://arxiv.org/abs/1412.6980, 2014. (Accessed 11 May 2023).
[68] M.R. Bonyadi, Z. Michalewicz, Particle swarm optimization for single objective continuous space problems: a review, Evol. Comput. 25 (1) (2017) 1–54, https://doi.org/10.1162/EVCO_r_00180.
[69] J. Kennedy, R. Eberhart, Particle swarm optimization, in: Proceedings of ICNN'95 - International Conference on Neural Networks vol. 4, 1995, pp. 1942–1948, https://doi.org/10.1109/ICNN.1995.488968. Perth, WA, Australia.
[70] E. Mezura-Montes, C.A.C. Coello, Constraint-handling in nature-inspired numerical optimization: past, present and future, Swarm Evol. Comput. 1 (4) (2011) 173–194, https://doi.org/10.1016/j.swevo.2011.10.001.
[71] M.E.H. Pedersen, Good Parameters for Particle Swarm Optimization, Hvass Lab., Copenhagen, Denmark, 2010, pp. 1551–3203. Tech. Rep. HL1001.
[72] B. Kamkari, D. Groulx, Experimental investigation of melting behaviour of phase change material in finned rectangular enclosures under different inclination angles, Exp. Therm. Fluid Sci. 97 (2018) 94–108, https://doi.org/10.1016/j.expthermflusci.2018.04.007.